J Eng Math (2010) 67:137–152
DOI 10.1007/s10665-009-9302-2

The flip-through of a plane inviscid jet with a free surface

Mark J. Cooker

Received: 28 August 2008 / Accepted: 8 June 2009 / Published online: 21 June 2009
© Springer Science+Business Media B.V. 2009

Abstract The growth of a two-dimensional liquid jet is modelled, in which an inviscid incompressible fluid is in irrotational flow. On the moving free surface, the pressure is constant. The flow is symmetric with respect to the y-axis. The free-surface fluid particle that lies on the y-axis is Q and it has position $y = Y(t)$. A velocity potential is presented that describes the local features of the flow near the centreline, and which contains essentially two unknowns: the velocity $V(t) = \mathrm{d}Y/\mathrm{d}t$ of Q, and a length $L(t)$. Near Q the free surface is a time-dependent parabola, whose curvature is directly proportional to a third unknown, $F(t)$. The kinematic and dynamic free-surface boundary conditions constrain V, L and F to satisfy three ordinary differential equations. The solutions are a one-parameter family that separate into five types. For one type the free-surface curvature changes sign during the motion, so that the free surface changes from concave to convex—it executes flip-through. Soon after flip-through, there is a local maximum in the pressure, with respect to time and space. A short time later there is a maximum in the acceleration of Q. As t tends to infinity, V tends to a constant, V_∞. An estimate is made of the time scale for flip-through, based on pressure changes, and it is found to decrease as V_∞ increases. When V_∞ is chosen very large, the values of the large maxima in pressure and acceleration become sensitive to small changes in the initial conditions. The results focus on the highly transient pressure field. The findings may help to describe the flip-through of a steep fronted water wave meeting a plane impermeable wall.

Keywords Flip-through · Hydrodynamic impact · Impact pressures · Inviscid jet

1 Introduction

The free surface of a liquid jet can move violently in several physically important settings. In the past, detailed computations of the free-surface flow of water waves breaking against a fixed vertical wall revealed the existence of narrow ascending jets with accelerations exceeding thousands of g. A jet emerges near the wall and ascends. An explanation of the very violent flow associated with such jets became a pre-occupation of Howell Peregrine until the end of his life. See for example Cooker and Peregrine [1] and Tuck [2]. Computations and analysis of jets arising from symmetric standing waves have also been reported by Longuet-Higgins [3] and Longuet-Higgins and

M. J. Cooker (✉)
School of Mathematics, University of East Anglia, Norwich, NR4 7TJ, UK
e-mail: m.cooker@uea.ac.uk

Dommermuth [4]. These flows can accompany high transient pressures within the fluid domain. In order to understand the high transient forces that breaking water waves exert on structures, we need to quantify the time-dependent pressure distribution on the solid boundary.

Shaped-charge devices are extreme examples of jets which are highly accelerated, and which attain high speeds of flight. Shaw et al. [5] photographed a jet travelling at 9,000 m/s along the axis of a conical charge only 0.06 m in diameter. The shaped charge was first modelled mathematically by Taylor [6]. A more detailed treatment is given by Birkhoff et al. [7]. Taylor modelled the flow that arises after the jet has emerged and lengthened enough for the neck and shoulder regions of the jet to be in steady flow. Steadily flowing jets are discussed in texts, e.g. [8, Chap. 9] and [9, Chap. 8]. But what conditions of *unsteady* flow prevail in the *early* stages of emergence of the shaped charge? It is during these earliest stages that the highest fluid pressures, (and the greatest rates of surface strain and relative displacement) are found. Cooker [10] has modelled the pressures at these earliest times of jet growth.

The influence of gravity in a jet that is falling under gravity, due to the Rayleigh–Taylor instability of an initially flat surface, is modelled by Duchemin et al. [11] and Duchemin [12]. They found that the tip of the jet has a slightly greater downward acceleration than g and that the tip curvature increases directly proportional to t^3.

Soon after the impact of a liquid drop, or a liquid wedge falling onto a plane rigid target, there are jets which emerge and spread quickly over the solid surface of the target. The jets are a source of difficulty in the analysis and computation of the flow. The fluid domain near the site of impact is greatly extended by the flow in the jet, and there are high velocities and accelerations of thousands of g to be accounted for in the early stages of motion. A computational difficulty in discretising the free surface is that small parts of the fluid domain quickly become elongated. Fluid particles that mark the computational free-surface position can become widely separated, and the free surface (and its velocity field) may become unacceptably poorly resolved.

Jets also occur during the entry of a solid body into water which is initially at rest. Contributions have been made to the theory of deep-water entry by Howison et al. [13], Fraenkel and McLeod [14] and by Semenov and Iafrati [15]. Deep-water entry is characterized by splash jets which ascend the sides of an impermeable body. By contrast, in sufficiently shallow water, the splash jets become detached from the body, because the root of each jet is swept away by the fluid that is forced out of the gap between the body and the bed. Korobkin [16] and Howison et al. [17] have accounted for this theoretically in two dimensions. Self-similar two-dimensional and axisymmetric flows for a crater collapsing and filling, in deep water, have been reported by Borisova et al. [18] and Zeff et al. [19]. Three-dimensional detached splashes have been computed by Roisman and Tropea [20] and Korobkin and Scolan [21]. The jet made by a collapsing enclosed cavity has been analysed by Longuet-Higgins and Oguz [22], who modelled the flow outside the cavity as that induced by a point sink traversing the interior of the cavity.

Recently Korobkin and Yilmaz [23], have modelled the early stages of flow when water is released from rest in a dam break: a jet emerges near the bed. A splash jet is made by the movement of a wavemaker or the wall of a container in the presence of gravity. King and Needham [24] showed, using small-time asymptotics, that a vertical section of wall, moving horizontally from rest with uniform acceleration into water, also initially at rest, induces an ascending splash-jet whose width and vertical displacement both grow from zero. The problem solved by King and Needham [24] involves an initial fluid domain which is a quarter-plane. A similar, but gravity-free flow, has been analysed by Shu [25], in which a uniformly accelerated wall moves into a fluid domain which is initially a truncated wedge of fluid at rest. Needham et al. [26] have treated the free-surface movement generated by an inclined accelerating plate, with gravity and surface tension, in water of fixed initial depth.

In this work we take a simple velocity potential that describes a local converging velocity field beneath a moving liquid surface. The velocity potential contains two functions to be determined. One function, $Y(t)$, is the position of the fluid particle Q on the y-axis of symmetry of the free surface, and the second function is a positive length scale $L(t)$. The upward velocity of Q is $V(t) = \mathrm{d}Y/\mathrm{d}t$. The dynamic free-surface boundary condition suggests that the free-surface shape near $x = 0$ is approximately parabolic, and the parabola is parameterised by $Y(t)$ and a further time-dependent shape factor, $F(t)$, which is the third function to be determined. The dynamic condition also forces V and L to satisfy two ordinary differential equations (ODEs) coupled with F. The kinematic boundary condition implies that F satisfies a third ODE which is coupled with V and L. The fourth condition is $V = \mathrm{d}Y/\mathrm{d}t$. In the presence of gravity the dynamical system has one non-zero equilibrium point. A linear stability analysis gives a

solution corresponding to standing waves of small amplitude. In the gravity-free limit, we solve a simplified system for V, L and F. There is a one-parameter family of solutions (parametrised by $F(0)$), which show distinct types of physical behaviour. We comment on the changes in the free-surface shape and the pressure distribution, particularly the high local maximum in pressure encountered in one type. We classify the solutions and identify some jet-like motions. The theory is valid for a fluid domain which extends from the free surface to $y = -\infty$, and both $|x|/L$ and $|F|x^2/L$ must be small enough for our power series to be valid approximations on the free surface. If we think of the y-axis as a vertical impermeable wall, then the theory describes the especially violent flow after the impact of a water wave against the wall.

We are most interested in the early development of the jet, while it is emerging with high acceleration. Compared with the pressure differences associated with the inertia of the flow, we can neglect capillary pressure differences across the free surface. For this reason we impose the condition that the fluid pressure vanishes at the free surface.

The results from this paper show that flows with unbounded acceleration are possible, but to achieve such flows the initial conditions must be specified with great precision. In practice there is a relatively narrow interval of the parameter $F(0)$ for which the peak pressure is as high as that encountered in wave impact experiments.

Some motivation for the starting point of the analysis below is two observations about the kind of velocity potential commonly encountered in water-wave studies. First, the velocity potential,

$$\phi = \phi_0 \exp(k[y - Y]) \cos(kx),$$

is a solution of Laplace's equation, even if ϕ_0, k and Y are all functions of time. Secondly the unit of velocity potential equals the unit of the coefficient ϕ_0, which is a speed $V(t)$ times a length $L(t)$. As explained in the sequel, it turns out to be kinematically necessary to choose $V(t) = \mathrm{d}Y/\mathrm{d}t$, (which in turn forces $\phi_0 = V/k$), and algebraically convenient to write $k(t) = 1/L(t)$.

The paper is organised as follows. The formulation of the governing differential equations, including gravity, is developed in Sect. 2. The solutions for gravity-free flows are worked out in parametric form in Sect. 3. In Sect. 4 we present some illustrative calculations and in Sect. 5 we draw together the conclusions.

2 Analysis

2.1 Preliminary analysis

The fluid is inviscid and incompressible with constant density ρ. The two-dimensional velocity field is irrotational and it is described by a velocity potential $\phi(x, y, t)$, where x, y are the usual Cartesian coordinates in an inertial frame of reference specified below, and t is time. A fluid particle, Q, lies on the free surface on the vertical line of symmetry which we impose on both the velocity and the initial fluid domain. The initial upward velocity of Q is ${V_0}^*$, where a starred quantity is dimensional. We take a time-dependent length scale, $L^*(t)$, which is initially ${L_0}^*$, associated with the distance over which the velocity field varies significantly from ${V_0}^*$. This leaves us free to choose arbitrarily the initial radius of curvature of the free surface at Q, discussed below.

The time t^* is scaled with respect to L_0^*/V_0^* and the pressure is scaled with respect to $\rho {V_0}^{*2}$. With respect to these dimensionless quantities, we consider the following dimensionless velocity potential, whose functional form was suggested by the observations at the end of the Introduction,

$$\phi(x, y, t) = V(t)L(t) \exp([y - Y(t)]/L(t)) \cos(x/L(t)), \tag{1}$$

where the dimensionless (unstarred) variables are $x = x^*/L_0^*$, $y = y^*/L_0^*$, the position of Q is $y = Y = Y(t)$, the speed of Q up the y-axis is $\mathrm{d}Y/\mathrm{d}t = V(t) = V^*(t^*)/{V_0}^*$ and $L(t) = L^*(t)/{L_0}^*$. These scalings force the initial data to be $L(0) = 1$, $Y(0) = 0$ (without loss of generality), and $V(0) = 1$. The fluid domain extends from the free surface down to $y = -\infty$, where the fluid is at rest. In the following the x-coordinate will be restricted such that $|x/L(t)|$ is small, so that in this sense the solution (1) is only *local*. But we will have within the fluid an unrestricted range for y from the free surface to $y = -\infty$.

Velocity potentials, different from (1) may also give rise to jet-like flows using the method discussed in this paper.

The fluid velocity is $\nabla\phi = u\mathbf{i} + v\mathbf{j}$, where, according to (1), the dimensionless velocity components are

$$u(x, y, t) = -V \exp([y - Y]/L) \sin(x/L), \tag{2}$$

$$v(x, y, t) = V \exp([y - Y]/L) \cos(x/L). \tag{3}$$

In Eq. (2), on $x = 0$, we have $u = 0$ and so the y-axis is a line of symmetry of the flow, and it is the axis of the jet. The point Q is at $x = 0$, $y = Y(t)$, and at Q (3) gives us $v = V(t) = \mathrm{d}Y/\mathrm{d}t$, so at Q the free-surface kinematic condition is satisfied. We anticipate the free surface passing through Q: the free surface is described by

$$y = Y(t) + \eta(x, t),$$

where we constrain η to vanish at $x = 0$. (The function $\eta(x, t)$ is expressed below, in (9).)

In (2) and (3), as $y \to -\infty$, the velocity components tend to zero exponentially quickly, if and only if $L(t) > 0$. In this sense the frame of reference in which (1) is expressed, is that of the water far below the free surface. Such an exponential decrease in u and v, as $y \to -\infty$, is found in the linear theory of water waves in deep water.

2.2 The free-surface position and the dynamic boundary condition

In dimensionless form Bernoulli's equation for the pressure, p, is

$$p = -\phi_t - \tfrac{1}{2}(u^2 + v^2) + \mathrm{Fr}^{-2}(Y - y) + p_\infty(t), \tag{4}$$

where the Froude number $\mathrm{Fr} = |V_0^*|(gL_0^*)^{-1/2}$, the acceleration due to gravity is g. Also $p_\infty(t)$ is a function of time such that, when $\mathrm{Fr}^{-2} = 0$, it equals the pressure at $y = -\infty$. The specification of $p_\infty(t)$ can be regarded as a far-field boundary condition. From (1) we find that

$$\begin{aligned} p = {} & \left(\left[V^2 - \frac{\mathrm{d}(LV)}{\mathrm{d}t} + V\frac{\mathrm{d}L}{\mathrm{d}t}\frac{(y - Y)}{L}\right]\cos\left(\frac{x}{L}\right) - V\frac{\mathrm{d}L}{\mathrm{d}t}\frac{x}{L}\sin\left(\frac{x}{L}\right)\right) \\ & \times \exp\left(\frac{y - Y}{L}\right) - \tfrac{1}{2}V^2\exp\left(\frac{2(y - Y)}{L}\right) - \mathrm{Fr}^{-2}(y - Y) + p_\infty. \end{aligned} \tag{5}$$

For points near Q, $|x/L| \ll 1$ and $|y - Y|/L \ll 1$. A Taylor-series expansion of (5) about Q gives

$$\begin{aligned} p = {} & \left(p_\infty - \frac{\mathrm{d}}{\mathrm{d}t}(LV) + \tfrac{1}{2}V^2\right) - (y - Y)\left(\frac{\mathrm{d}V}{\mathrm{d}t} + \mathrm{Fr}^{-2}\right) \\ & + \frac{x^2}{2L^2}\left(L\frac{\mathrm{d}V}{\mathrm{d}t} - V\frac{\mathrm{d}L}{\mathrm{d}t} - V^2\right) + \frac{(y - Y)^2}{2L^2}\left(V\frac{\mathrm{d}L}{\mathrm{d}t} - L\frac{\mathrm{d}V}{\mathrm{d}t} - V^2\right) \\ & + \frac{x^4}{4!L^4}\left(3V\frac{\mathrm{d}L}{\mathrm{d}t} - L\frac{\mathrm{d}V}{\mathrm{d}t} + V^2\right) + \frac{x^2(y - Y)}{2L^3}\left(L\frac{\mathrm{d}V}{\mathrm{d}t} - V\frac{\mathrm{d}L}{\mathrm{d}t} - V^2\right) \\ & + O([y - Y]^3/L^3, [y - Y]^2x^2/L^4, [y - Y]x^4/L^5, x^6/L^6). \end{aligned} \tag{6}$$

Now $p = 0$ on the free surface, which lies at $y = Y + \eta(x, t)$, so that (6) gives

$$\begin{aligned} 0 = {} & \left(p_\infty - \frac{\mathrm{d}}{\mathrm{d}t}(LV) + \tfrac{1}{2}V^2\right) - \eta\left(\frac{\mathrm{d}V}{\mathrm{d}t} + \mathrm{Fr}^{-2}\right) \\ & + \frac{x^2}{2L^2}\left(L\frac{\mathrm{d}V}{\mathrm{d}t} - V\frac{\mathrm{d}L}{\mathrm{d}t} - V^2\right) + \frac{\eta^2}{2L^2}\left(V\frac{\mathrm{d}L}{\mathrm{d}t} - L\frac{\mathrm{d}V}{\mathrm{d}t} - V^2\right) \\ & + \frac{x^2\eta}{2L^3}\left(L\frac{\mathrm{d}V}{\mathrm{d}t} - V\frac{\mathrm{d}L}{\mathrm{d}t} - V^2\right) + \frac{x^4}{4!L^4}\left(3V\frac{\mathrm{d}L}{\mathrm{d}t} - L\frac{\mathrm{d}V}{\mathrm{d}t} + V^2\right) \\ & + O(\eta^3/L^3, \eta^2x^2/L^4, \eta x^4/L^5, x^6/L^6). \end{aligned} \tag{7}$$

At Q we have $x = 0$ and $\eta = 0$, and the pressure is zero, so the first term on the RHS of (7) must vanish. Hence

$$\frac{\mathrm{d}}{\mathrm{d}t}(LV) - \tfrac{1}{2}V^2 = p_\infty(t). \tag{8}$$

Suppose, for a moment, that η/L and x/L are of the same order of magnitude. Then the lowest-order term on RHS (the right-hand side) of (7) is the second term. So at first-order $\mathrm{d}V/\mathrm{d}t = -\mathrm{Fr}^{-2}$. Therefore Q can move upward but with only constant deceleration, i.e., in free-fall, which is uninteresting. Besides, if η is directly proportional to x, the free surface is a straight line and not jet-like.

We now reconsider the RHS of (7) and assume that the second and third terms balance each other, so that η is directly proportional to x^2. Then the other terms displayed in (7) are $O(x^4/L^4)$ and therefore negligible for small $|x|/L$. Then the symmetric free surface position must have the form

$$y = Y + \eta(x,t) = Y + x^2F(t) + O(x^4/L^4), \tag{9}$$

where $F(t)$ is a new unknown in the theory. At $O(x^2/L^2)$ in (7) we find that

$$2FL^2\frac{\mathrm{d}V}{\mathrm{d}t} + 2FL^2\mathrm{Fr}^{-2} + V\frac{\mathrm{d}L}{\mathrm{d}t} - L\frac{\mathrm{d}V}{\mathrm{d}t} + V^2 = 0. \tag{10}$$

2.3 The free-surface kinematic condition

The kinematic condition on $y = Y + \eta(x,t)$ is

$$V + \eta_t + \phi_x\eta_x = \phi_y. \tag{11}$$

With the help of definition (9), we make a Taylor-series expansion about Q, for suitably small Fx^2/L, so that (11) becomes

$$\begin{aligned} &V + x^2\frac{\mathrm{d}F}{\mathrm{d}t} - 2xFV(1 + Fx^2/L + O(F^2x^4/L^2))(x/L + O(x^3/6L^3)) \\ &\quad = V(1 + Fx^2/L + O(F^2x^4/L^2))(1 - x^2/2L^2 + O(x^4/24L^4)), \end{aligned} \tag{12}$$

which implies

$$\frac{x^2}{L^2}\left(L^2\frac{\mathrm{d}F}{\mathrm{d}t} - 3FLV + \frac{V}{2}\right) + O(x^4L^{-4}) = 0.$$

Hence at $O(x^2/L^2)$ we must have

$$\frac{\mathrm{d}F}{\mathrm{d}t} = \frac{3FV}{L} - \frac{V}{2L^2}. \tag{13}$$

Equations (8), (10), (13) and $\mathrm{d}Y/\mathrm{d}t = V$ are four coupled ordinary differential equations for V, L, F, Y. We recast these equations into the form of a dynamical system by eliminating first $\mathrm{d}L/\mathrm{d}t$ from (8) and then $\mathrm{d}V/\mathrm{d}t$ from (10):

$$\frac{\mathrm{d}V}{\mathrm{d}t} = \frac{3V^2 + 2p_\infty}{4L(1-FL)} + \mathrm{Fr}^{-2}\left(\frac{FL}{1-FL}\right), \tag{14}$$

$$\frac{\mathrm{d}L}{\mathrm{d}t} = \frac{p_\infty(1-2FL) - \frac{1}{2}V^2(1+2FL)}{2V(1-FL)} - \mathrm{Fr}^{-2}\frac{FL^2}{V(1-FL)}, \tag{15}$$

$$\frac{\mathrm{d}F}{\mathrm{d}t} = \frac{3FV}{L} - \frac{V}{2L^2}, \tag{16}$$

$$\frac{\mathrm{d}Y}{\mathrm{d}t} = V, \tag{17}$$

where $FL \neq 1$. In this set of equations there is no explicit dependence on Y so Eq. (17) is needed only to find Y from V and (14–16) is a system of three equations in the three unknowns V, L, F.

The fluid domain is a semi-infinite vertical strip from the free-surface downwards, so that $y \le Y(t) + Fx^2$. We have assumed that $|x|/L$ is small, and we assume that $F(t)$ and $L(t)$ are such that $|F|x^2/L \ll 1$. Since we are interested in motions for which F passes through 0, and because L is positive, we can be confident of some time interval during which $|F|x^2/L \ll 1$. This last condition is violated if L decreases to zero.

There is one equilibrium point for the system (14–17). This lies at $V = 0$, $Y = 0$, $F = 0$, and $L = 1$. This corresponds to static fluid with a plane horizontal free surface. There are small-amplitude oscillations about the equilibrium point. In order to be able to carry out a linear stability analysis we must desingularize the right-hand side of (15) at $V = 0$ by choosing $p_\infty = 2\mathrm{Fr}^{-2}F$. Then the linear solution with respect to small values of ϵ, is such that the displacement of Q is $Y = \epsilon \sin\omega t$, its velocity is $V = \epsilon\omega\cos\omega t$, the positive length scale $L = 1 - \frac{1}{4}\epsilon\omega\cos\omega t$, and the free-surface curvature function $F = -\frac{1}{2}\epsilon\sin\omega t$. Consequently, the quantity $p_\infty = -\mathrm{Fr}^{-2}\epsilon\sin\omega t$. Also the dimensionless dispersion relation is $\omega^2 = \mathrm{Fr}^{-2}$.

This linear solution corresponds to a standing water wave whose free surface (in dimensionless quantities) is $y = \epsilon\sin\omega t\cos kx$. Here k equals the time-average of L^{-1}, namely unity. So the familiar dimensional dispersion relation $\omega^{*2} = gk^*$ is the same as $\omega^2(V_0^*/L_0^*)^2 = g/L_0^*$, which is the dimensionless relation $\omega^2 = \mathrm{Fr}^{-2}$.

The full dynamical system (14–17) is complicated by the function $p_\infty(t)$, which must be chosen as part of the far-field boundary conditions. From now on we choose $p_\infty(t) = 0$, so that the pressure in (5) decreases to zero exponentially quickly as $y \to -\infty$. Hence the nett fluid force on the y-axis is finite. The system (14–17) is also made complicated by gravity, through the Froude-number dependence of the coefficient Fr^{-2} in (14) and (15). From now on we study the large-Froude-number limit appropriate to very violent motions in which the free-surface particle acceleration V_0^{*2}/L_0^* is much greater than g so that Fr^{-2} is negligible. Hence we have a dynamical system for V, L and F:

$$\frac{\mathrm{d}V}{\mathrm{d}t} = \frac{3V^2}{4L(1-FL)}, \quad \frac{\mathrm{d}L}{\mathrm{d}t} = -\frac{V(1+2FL)}{4(1-FL)}, \quad \frac{\mathrm{d}F}{\mathrm{d}t} = \frac{V(6FL-1)}{2L^2}. \tag{18, 19, 20}$$

The initial conditions are $V(0) = 1$, $L(0) = 1$, and $F(0) = F_0$, which can take any real value not equal to unity. So this problem has only one parameter, F_0. In the next section we solve the system of equations, and we end this section with a comment on the above procedure.

The above model equations were derived for a limited set of unknowns, by expanding, in powers of x and y, the dynamic and kinematic boundary conditions. This procedure might (incorrectly) be thought to be equivalent to taking a general velocity potential

$$\phi(x, y, t) = a_0(t) + a_1(t)[y - Y] + a_2(t)(x^2 - [y - Y]^2) + a_3(t)([y - Y]^3 - 3x^2[y - Y]) + \cdots, \tag{21}$$

where $\partial\phi/\partial x = 0$ at $x = 0$. Here each term satisfies Laplace's equation, and has a coefficient $a_i(t)$ to be determined. However, such an approach fails because the system of equations for $\{a_i(t)\}$ cannot be closed: one always has more unknowns than conditions at every order of truncation.

3 Solutions

3.1 Expressions for V, L, F, Y, t in terms of parameter w

Equations (18) to (20) are a nonlinear autonomous dynamical system. We will eliminate t and then find V, L and F in terms of a parameter $w = FL$. At the end we will find t and Y in terms of w by using (17).

Dividing (20) by (19) we have

$$\frac{\mathrm{d}F}{\mathrm{d}L} = \frac{2(6FL-1)(FL-1)}{L^2(1+2FL)}, \tag{22}$$

in which the prevalence of FL prompts us to substitute $F = w/L$. Equation (22) implies

$$L\frac{\mathrm{d}w}{\mathrm{d}L} = \frac{14w^2 - 13w + 2}{2w + 1}, \tag{23}$$

which is a separable differential equation. At $t = 0$, $L(0) = 1$, and so thinking of w as a function of time, we have $w(0) = F_0$, for the lower limit of integration in

$$\log|L| = \int_{F_0}^{w} \frac{2w' + 1}{14(w' - a)(w' - b)}\,\mathrm{d}w', \tag{24}$$

where we define the roots of the quadratic in the numerator of (23) as

$$a = \frac{13 + \sqrt{57}}{28} = 0.733923 \quad \text{and} \quad b = \frac{13 - \sqrt{57}}{28} = 0.194649.$$

Evaluating the integral by partial fractions gives us the parametric solution for $L(w)$:

$$L(w) = \left|\frac{w - a}{F_0 - a}\right|^{q_1} \left|\frac{F_0 - b}{w - b}\right|^{q_2}, \tag{25}$$

where $F_0 \neq a$, $F_0 \neq b$ and $w \neq b$, and we define the constants

$$q_1 = \frac{1}{14} + \frac{27}{14^2(a - b)} = 0.326874, \quad q_2 = -\frac{1}{14} + \frac{27}{14^2(a - b)} = 0.184017.$$

Since $F = w/L$, we have also

$$F(w) = w\left|\frac{F_0 - a}{w - a}\right|^{q_1} \left|\frac{w - b}{F_0 - b}\right|^{q_2}. \tag{26}$$

By dividing (18) by (19) and carrying out a similar analysis, we obtain

$$V(w) = \left|\left(\frac{F_0 - a}{w - a}\right)\left(\frac{w - b}{F_0 - b}\right)\right|^{q_3}, \tag{27}$$

where initially $w = F_0$ and $V = 1$, and where $q_3 = \frac{3}{14(a-b)} = 0.397360$.

We anticipate the discussion below with a pair of results. If $F_0 : 0 < F_0 < b$ or $F_0 > 1$ then as $|w| \to \infty$, (27) implies that V tends to a constant V_∞, where

$$V_\infty = \left|\frac{a - F_0}{b - F_0}\right|^{q_3}. \tag{28}$$

This equation allows us to choose F_0 so as to achieve a given positive value of V_∞. Inverting (28) gives

$$F_0 = \frac{b{V_\infty}^{1/q_3} - a}{{V_\infty}^{1/q_3} - 1}.$$

We complete the set of parametric solutions by expressing Y and t in terms of w. Dividing (17) by (18) gives us

$$\frac{\mathrm{d}Y}{\mathrm{d}V} = \frac{4(1 - w)L(w)}{3V(w)}, \tag{29}$$

and we can use the w-derivative of the logarithm of (27) to write $\mathrm{d}V/V$ in terms of $\mathrm{d}w$ and w. Separating out the variables of Eq. (29), and integrating, gives

$$Y = \frac{2|F_0 - b|^{q_2}}{7|F_0 - a|^{q_1}} \int_{F_0}^{w} \frac{w' - 1}{|w' - a|^{1-q_1}|w' - b|^{1+q_2}}\,\mathrm{d}w', \tag{30}$$

in which the exponents $1 - q_1 = 0.6730$ and $1 + q_2 = 1.184$ are positive, and the limits are such that at $t = 0$, $Y(0) = 0$ and $w = F_0$. From (17) and (30) the time t is related to w by

$$t = \frac{2|F_0 - b|^{q_2+q_3}}{7|F_0 - a|^{q_1+q_3}} \int_{F_0}^{w} \frac{w' - 1}{|w' - a|^{1-q_1-q_3}|w' - b|^{1+q_2+q_3}}\,\mathrm{d}w', \tag{31}$$

where the displayed exponents $1 - q_1 - q_3 = 0.2758$ and $1 + q_2 + q_3 = 1.581$ are positive.

For the RHS of (31) to be time-like we must arrange for w to belong to an interval, I, with F_0 at one of the end-points of I. Also w must either increase or decrease from F_0 in such a way that t increases from zero. The integrand of (31) has a singularity at $w = a$, which is also a singularity for F and V in finite time. In (31) the exponent $1 + q_2 + q_3 = 1.581$ is greater than one, so the singularity at $w = b$ is not integrable. Hence we may only let w move away from b, on the same side of b as that on which F_0 lies, in order that $t \geq 0$.

The above considerations help us to identify four types of interval, I, which capture all the admissible real values which might be chosen for F_0, not equal to a or b:

(i) If $F_0 : F_0 > 1$ then $I = [F_0, \infty)$, in which w is increasing from F_0 and $t : 0 \leq t < \infty$;
(ii) If $F_0 : a < F_0 < 1$, then $I = (a, F_0]$, where w decreases from F_0 to a, and $t : 0 \leq t < T$, where $T > 0$ is finite;
(iii) If $F_0 : b < F_0 < a$, then $I = (b, F_0]$, in which w is decreasing from F_0 towards b, and $t : 0 < t < \infty$;
(iv) If $F_0 < b$ then $I = (-\infty, F_0]$ in which w is decreasing from F_0 and $t : 0 \leq t < \infty$.

All the above intervals are extended in obvious ways to obtain $t < 0$.

Both of the integrals in (30, 31) can be written in terms of Incomplete Beta Functions, but these are slow to evaluate, even by computer. It is more useful (in support of the later analysis) to approximate them with elementary functions. We are particularly interested in case (iv), when $F_0 < b$, and $w' \leq b$. In (31) the integrand has the factor $(a - w')^{-1+q_1+q_3}$, which is a very slowly varying function of $w' < b$, compared with the other factors. So we expand it in a series of powers of $(b - w')$. As w' tends to $-\infty$ the integrand of (31) tends to zero in a way that is well-approximated by $(1-w')^{q_1-q_2-1}$. Integrating the sum of these two asymptotic terms gives us an approximation with a relative error of less than four per cent for the working range of $w < b$:

$$t \approx \frac{2(b - F_0)^{q_2+q_3}}{7(a - F_0)^{q_1+q_3}} \left(\frac{1 - b}{(q_2 + q_3)(a - b)^{q_4}} \left[\frac{1}{(b - F_0)^{q_2+q_3}} - \frac{1}{(b - w)^{q_2+q_3}} \right] + \frac{1}{q_1 - q_2} [(1 - w)^{q_1-q_2} - (1 - F_0)^{q_1-q_2}] \right). \tag{32}$$

where $q_4 = 1 - q_1 - q_3$. A similar treatment of (30) gives an approximation for Y:

$$Y \approx \frac{2(b - F_0)^{q_2}}{7(a - F_0)^{q_1}} \left(\frac{1 - b}{q_2(a - b)^{1-q_1}} \left[\frac{1}{(b - F_0)^{q_2}} - \frac{1}{(b - w)^{q_2}} \right] + \frac{\alpha}{q_1 - q_2} [(\beta - w)^{q_1-q_2} - (\beta - F_0)^{q_1-q_2}] \right), \tag{33}$$

where $\alpha = 0.6$ and $\beta = 4$ were found (by trials) to give a relative error of less than six per cent spread conveniently over the range of $w : 25 < w < b$ used in the results for this paper.

Figure 1 shows $V(t)$ plotted using (27), and (32) for $V_\infty = 2$ and 4. The plot shows that the acceleration is briefly large and that V tends more quickly to V_∞ when $V_\infty = 4$ than for $V_\infty = 2$.

3.2 Classification of solutions

We have found that L changes only a little from unity as $t \to \infty$, so we ignore results for L and plot in Fig. 2 a projection of the three-dimensional V, F, L phase space onto the V, F plane. In Fig. 2 all of the phase trajectories begin at the start line $V = 1$, each with its own value of F_0. As time increases V changes monotonically from unity, so one can 'read' along each phase curve.

Depending on the value of F_0, the solutions fall into Types I to V, defined as follows:

Type I. If $F_0 > 1$ then V *decreases* from unity as t increases, according to (25) and (27), $L \to \infty$ and $F \to \infty$. Physically, the two halves of the free surface, on either side of Q, close slowly towards each other. While this occurs Q slows down to a constant speed given by (28). See the dotted curves in Fig. 2.

Type II. If $F_0 : a < F_0 < 1$, then w decreases towards a, with increasing $t < T$. As $t \to T$ we have $L \to 0$, $F \to \infty$ and $V \to \infty$. Physically, the two halves of the free surface clap together in a finite time, which from

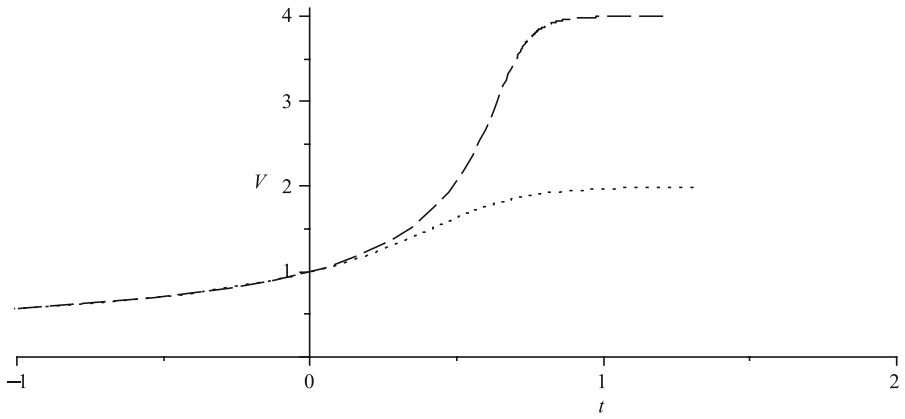

Fig. 1 The velocity, V, of the nose Q of the jet, plotted as a function of time. As $t \to \infty$, $V \to V_\infty$. The curves are drawn for $\cdots\ V_\infty = 2$ and $---\ V_\infty = 4$

(31) is approximately $T = 2(1-a)(F_0-b)^r/(7r[a-b]^{r+1})$, where $r = q_2+q_3$. The trajectories of Type II fly off the upper right corner of Fig. 2. These have little physical relevance because of the vanishing (as $L \to 0$) of the range of x within which the approximations are valid.

Type III. If $F_0 : b < F_0 < a$, then, as w decreases towards b, with ever increasing t, we have $L \to \infty$, $F \to 0$ and $V \to 0$. Physically, the free surface moves ever slower and becomes ever flatter. In Fig. 2 the trajectories (solid curves) converge on the origin.

Type IV. If $F_0 : 0 < F_0 < b$ then F initially increases, to a maximum positive value, and then decreases. Then F *changes sign* from positive to negative. As $t \to \infty$, F tends to $-\infty$, and V increases to a finite limiting value of $V_\infty > 1.695$ as given by (28). The long dashed curves in Fig. 2 are the trajectories that cross the V-axis, and these correspond to flip-through.

Type V. If $F_0 < 0$ then F tends to $-\infty$, and $L \to \infty$, while V is increasing from unity to a limiting value $V_\infty > 1$ given by (28). These limiting conditions are approached as $t \to \infty$. Type V corresponds to a jet whose free surface starts convex and stays convex. The jet curvature at Q tends to $-\infty$, and V increases to some value of V_∞ between 1 and 1.695. These are the dash-dot curves in the lowest part of Fig. 2.

The importance of Type IV lies in the change in sign of F. Hence the curvature, $2F$, at Q changes sign, and so the free surface parabola passes from concave to convex. In Type IV solutions, the free surface executes flip-through. In Fig. 2, three Type IV curves are drawn, showing F changing sign. Figures 3 and 4 show examples of flip-through. The parabolic free surface is shown at several times as Q accelerates upward and the free surface changes from concave to convex.

The rarity of Type IV, among the flows discussed here, reflects how special the initial conditions must be to bring about a flip-through. A similar sensitivity has been reported by experimentalists. There are records of field measurements of thousands of consecutive waves meeting a seawall where none registers a significant pressure, before one incident wave possesses the right conditions to make a high-pressure impact. Sensitivity to incident wave conditions was reported for example, in the wave-tank experiments of Bagnold [27]. He generated disturbances that were close to solitary waves, with the aid of a carefully controlled paddle wavemaker. In [27, p. 211] Bagnold states that the conditions to achieve an impact were so critical that: "an alteration of but 0.2% in the paddle timing was sufficient to make the pressures disappear altogether." He also commented on the influence of free-surface roughness which can increase or diminish the peak pressures. Such irregular wave features at the waterline could alter significantly the free-surface curvature.

So far we have investigated all real values of $F_0 \neq 1$, except $F_0 = a$ (which is the border between Types II and III) and $F_0 = b$ (the borderline case between Types III and IV). For these values the parametric solution method fails because $FL = w$ does not then describe a time-like variable. Instead FL is a constant which equals F_0 (= a or

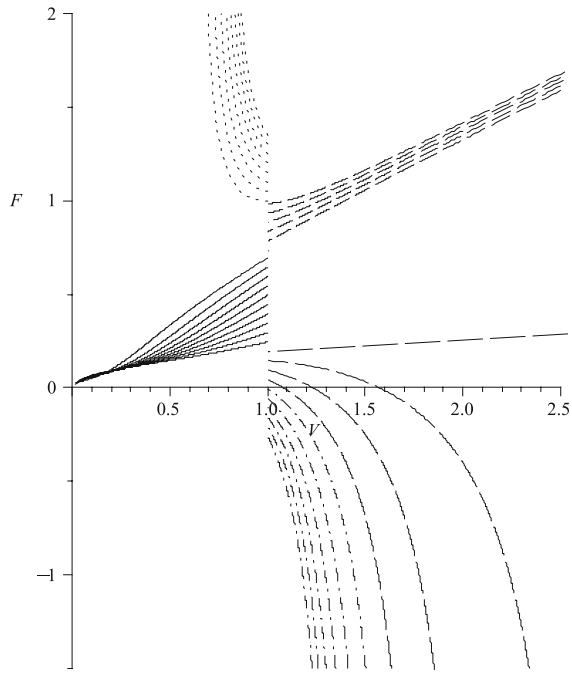

Fig. 2 Solution curves in the V, F plane, Eqs. (26) and (27). At $t = 0$, $V = 1$ and $F = F_0$ where F_0 parametrizes the solutions. Results for $-0.27 < F_0 < 1.42$ only are drawn. Each curve begins at the initial line $V = 1$, from which the curve can be read forward in time. From top to bottom of the plot the curves are: $\cdots$ for Type I solutions, $F_0 > 1$, for which V decreases as t increases. Curves – – – are Type II in which $F_0 : a < F_0 < 1$, where $a = 0.733923$: here the two halves of the free surface clap together in finite time. Curves — are Type III solutions $F_0 : b < F_0 < a$ (where $b = 0.194649$) and these slowly approach the origin. Curves — — — are Type IV, flip-through, solutions, for $F_0 : 0 < F_0 < b$, where F changes sign. Curves – · – · – are for Type V solutions, $F_0 < 0$, in which F remains negative and the free surface is convex for $t > 0$

b only). The system (18–20) then possesses a similarity solution such that $F = F_0 V^s$ where $s = (1 + 2F_0)/3$ and where

$$V = \left(1 - \frac{t}{T}\right)^{-3/(4+2F_0)} \quad \text{where} \quad T = \frac{2(1 - F_0)}{2 + F_0}. \tag{34}$$

The expression for V is valid for $t : 0 \le t < T$, but V and F are singular at the critical time $t = T$. In this flow as $t \to T$ we find that $L = F_0/F \to 0$ and $Y \to Y_T = 4(1 - F_0)/(1 + 2F_0)$.

Physically the two halves of the free surface come together above Q, and this happens while Q rises a finite distance from $y = 0$ to $y = Y_T$. For time $t < T$ the maximum pressure rises without bound, but the model breaks down at $t = T$ and it is unable to predict any of the probably very violent flow conditions for $t \ge T$. These two self-similar solutions rely on particular values of F_0, and so are of little importance in the continuum of results within each of the Types I–V.

Since they correspond to flip-through, in the rest of the paper we concentrate on Type IV solutions $F_0 : 0 < F_0 < b$. As w passes through zero, from positive to negative values, Eq. (26) shows that F also passes through zero from positive to negative. Hence the free surface changes from a concave crater into a convex jet. The expression (25) shows that L decreases slowly from unity, and V increases continually towards V_∞, as w tends to $-\infty$ in Eq. (27). By choosing F_0 close to b, Eq. (28) shows that V_∞ can be made very large.

3.3 The free surface: its motion and change of shape

So far we have treated the motion as an initial-value problem but we are free to consider time $t < 0$ too. It has been shown that the exact result (26) gives us the shape factor, F, in the expression for the free surface $y = Y(t) + F(t)x^2$. For Y we have Eq. (30), which depends (through F_0) on the chosen value of V_∞. For $Y \to -\infty$, (i.e., $t \to -\infty$) we find that $F > 0$ and decreasing to zero. So the free surface is concave and close to flat for sufficiently large and negative Y (or t).

As t increases from $-\infty$, Y increases monotonically from $-\infty$ to ∞, and V increases monotonically from zero to V_∞; see Fig. 1. In (26) and (27), as w increases to b we have F increasing from zero to a positive maximum, and then later decreasing. The local maximum in F occurs when $\mathrm{d}F/\mathrm{d}t = 0$, which is equivalent to $\mathrm{d}F/\mathrm{d}w = 0$, and this implies that $w = 1/6$, uniquely. Hence the local maximum value of F for Type IV motion is

$$F_{\max} = \frac{1}{6}\left|\frac{a - F_0}{a - 1/6}\right|^{q_1}\left|\frac{b - 1/6}{b - F_0}\right|^{q_2}. \tag{35}$$

When $w = 1/6$, Eqs. (27, 28) show that the value of V has increased to $0.3025\,V_\infty$. The maximum in F corresponds to the instant that the radius of curvature $R = 1/(2F)$ of the concave free surface at Q achieves its smallest value $R_{\min}$ equal to $(2F_{\max})^{-1}$. After this instant the free surface becomes less concave, and then becomes momentarily flat, when F and w both vanish. This is the instant of flip-through. It occurs when $V = V_f = V_\infty[b/a]^{q_3} = 0.5901\,V_\infty$. At later times the free surface is convex with a jet-like shape and ascent. The nose of the jet has ever greater convex curvature as time goes on. Figures 3 and 4 show the flip-through of the free surface for two values of V_∞. For $V_\infty = 4$ in Fig. 4, the transition is quicker and produces a sharper jet than for the case $V_\infty = 2$ drawn in Fig. 3.

As t tends to infinity we have $w \to -\infty$ in (26) and (31) and from these we find that the curvature $2F$ is asymptotically directly proportional to $t^{7(1-q_1-q_2)}$ where $7(1 - q_1 - q_2) = 3.423$. Duchemin et al. [11] and Duchemin [12] found that for jets drawn downwards by gravity, the tip curvature is asymptotically proportional to t^3.

After flip-through, V carries on increasing towards V_∞. On the way, two more important events occur, which we discuss next: first a peak in the spatial maximum in pressure and a little later the maximum acceleration of the nose of the jet.

3.4 The time-dependent pressure distribution

In the problem of wave impact we can replace the y-axis by an impermeable wall and consider first the pressure distribution at $x = 0$. On the y-axis, below Q, Eq. (6) gives the pressure as

$$p(0, y, t) = (Y - y)\frac{\mathrm{d}V}{\mathrm{d}t} - \frac{(Y - y)^2}{2L^2}\left(L\frac{\mathrm{d}V}{\mathrm{d}t} - V\frac{\mathrm{d}L}{\mathrm{d}t} + V^2\right) + O\left(\frac{Y - y}{L}\right)^3,$$

where $y \le Y$. Using (18–20), we may simplify this to

$$p(0, y, t) = \frac{V^2}{1 - w}\left(\frac{3(Y - y)}{4L} - (1 - \frac{1}{4}w)\frac{(Y - y)^2}{L^2}\right) + O\left(\frac{Y - y}{L}\right)^3. \tag{36}$$

For any one value of F_0, at any fixed time t, the pressure on the y-axis has a spatial maximum of magnitude $p_{\max}(t)$. This maximum lies at a position that we denote $y = y_{\max}$. Elementary algebra gives

$$y_{\max} = Y(w) - \frac{3L(w)}{8 - 2w}, \tag{37}$$

and

$$p_{\max} = \frac{9}{8(1 - w)(8 - 2w)}\left(\frac{b - w}{a - w}\right)^{2q_3}\left(\frac{a - F_0}{b - F_0}\right)^{2q_3}. \tag{38}$$

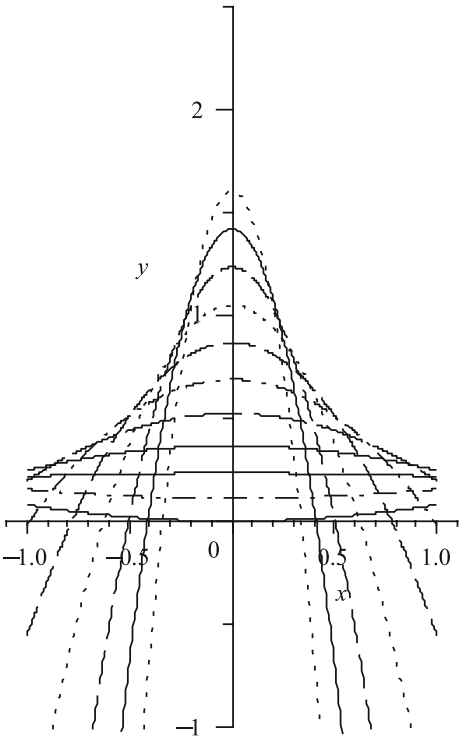

Fig. 3 Flip-through: motion of the parabolic free surface for $V_\infty = 2$. The surface accelerates up and flips through when the surface is instantaneously flat. Times shown: $t = 0$ (*lowermost* curve) to $t = 1.0$ (*uppermost* curve), in time-increments of 0.1. The x- and y-axes are scaled the same

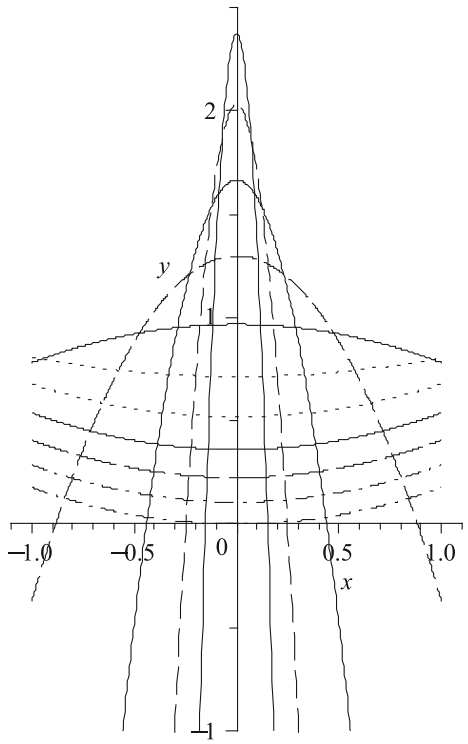

Fig. 4 As Fig. 3: free-surface positions for $V_\infty = 4$. The surface flips-through when it is instantaneously flat. Times shown: $t = 0$ (*lowest* curve) to $t = 1.0$ (*uppermost* curve), in time-increments of 0.1. The x- and y-axes are scaled the same

For fixed F_0 the global maximum value of $p_{\max}$ occurs when the w-derivative of (38) vanishes. This turns out to imply that w must satisfy a cubic equation, the one root of which that is less than b is $w = w_p = -0.229155$, independent of F_0. The corresponding maximum of $p_{\max}(t)$, which we call the 'peak pressure', is denoted $p_{\rm pk}$, where

$$p_{\rm pk} = 0.05637\,\frac{(a - F_0)^{2q_3}}{(b - F_0)^{2q_3}} = 0.05637\,{V_\infty}^2. \tag{39}$$

The peak pressure tends to infinity as V_∞ tends to infinity, and this occurs as F_0 increases to b, corresponding to a critical initial radius of curvature $R = R_c = 1/(2b) = 2.569$.

Equation (37) gives us the vertical distance, D, from the position of maximum pressure up to the point Q on the free surface:

$$D(w) = Y - y_{\max} = \frac{3}{8 - 2w}\left(\frac{a - w}{a - F_0}\right)^{q_1}\left(\frac{b - F_0}{b - w}\right)^{q_2}. \tag{40}$$

At the time of peak pressure, $w = w_p$, and the corresponding value of D is D_p where:

$$D_p = 0.4103\,\frac{(b - F_0)^{q_2}}{(a - F_0)^{q_1}}. \tag{41}$$

Equations (39) and (41) show that as F_0 tends to b from below, $p_{\rm pk}$ tends to infinity and D_p tends to zero.

In Fig. 5 the pressure distribution on the y-axis is plotted at several times for $V_\infty = 4$ (corresponding to $F_0 = 0.1776$, which is slightly less than $b = 0.1946$). At the right-most point of the pressure distribution the

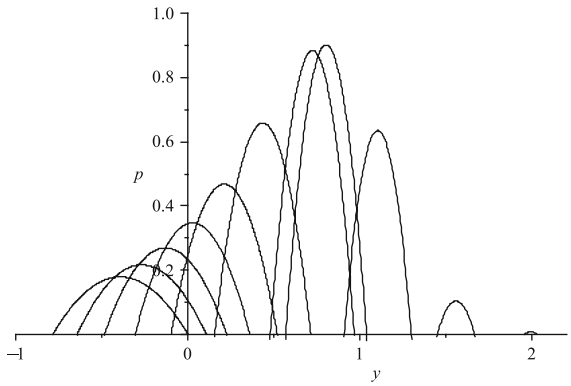

Fig. 5 The pressure distribution on the y-axis at several instants. The spatial maximum in pres sure is at a point $y = y_{\max}$ which ascends (moves to the right in this plot). The point where $p = 0$, at the right-hand end of each curve, coincides with the instantaneous position of the free surface on the y-axis. The spatial maximum pressure, $p_{\max}$, attains its greatest value, $p_{\rm pk}$, for one of the curves plotted. This plot is made for $V_\infty = 4$, for which $p_{\rm pk} = 0.9019$. In dimensional units $p_{\rm pk} = 0.9019\,\rho V_0^{*2}$, where $V_0{}^*$ is the dimensional initial speed of P. Times shown are $t = 0$ (*leftmost* curve) to $t = 0.9$ (*rightmost* curve), in time-increments of 0.1, and for $t = 0.5739$ which is the instant of peak pressure

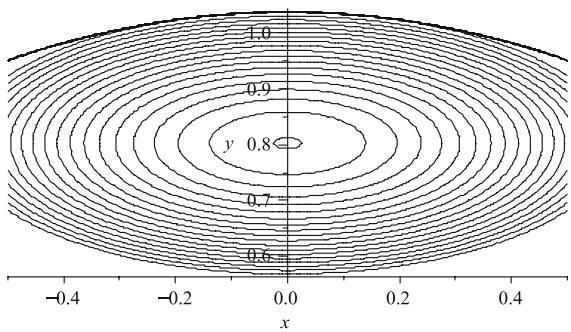

Fig. 6 Contour map of the pressure from (42), in the x, y-plane, at the instant of peak pressure, for $V_\infty = 4$. The pressure distribution is symmetric about the y-axis. The contours drawn are $p = 0\,[0.05]\,0.90$, where $p = 0$ is the outermost contour. The x- and y-axes are scaled the same. The thick *uppermost* curve is the parabolic free surface. This is close to the contour $p = 0$ for $-0.3 \le x \le 0.3$, which indicates the interval of x within which the approximations made are accurate

pressure is zero at Q and Q advances to the right. As time increases, the local spatial maximum in pressure increases to its temporal maximum and later decreases. In this example the peak pressure is $p_{\rm pk} = 0.9019$. In starred, dimensional units this pressure is $p_{\rm pk}{}^* = 0.9019\rho V_0{}^{*2}$, where $V_0{}^*$ is the dimensional initial speed of Q, and $V_\infty{}^* = 4V_0{}^*$.

Figure 6 shows the pressure distribution in x, y-space at the instant of peak pressure, for $V_\infty = 4$. The local maximum is prominent and coincides with the highest curve of pressure drawn in Fig. 5. In (6) the pressure is approximated by terms quadratic in the coordinates. Using (18–20), we may write (6) as follows,

$$p = \frac{V^2(4-w)}{4(1-w)}\left(\frac{3w}{(4-w)}\frac{x^2}{L^2} - \left[\frac{Y-y}{L} - \frac{3}{8-2w}\right]^2 + \frac{9}{(8-2w)^2}\right), \tag{42}$$

where V, Y, L are known functions of w. The time of greatest maximum pressure coincides with $w = w_p = -0.229155$, and for this instant contours of constant pressure from (42) are plotted in Fig. 6. The figure also shows the instantaneous free-surface position. The free surface is close to the $p = 0$ contour for $x : -0.3 < x < 0.3$, and within this interval the theory provides an adequate approximation.

As time goes on, the pressure distribution in (x, y) space changes its character. While the free surface is concave ($w > 0$ in (42)), the pressure contours are hyperbolas and the stationary point in pressure is a saddle point

(a maximum with respect to y and a minimum with respect to x). Mid-way through flip-through when $F = 0$ (and $w = 0$) the pressure contours are instantaneously horizontal. Only thereafter, when the surface becomes convex ($w < 0$), does the pressure possess a local maximum in space, and the maximum is surrounded by elliptical contours.

For values of V_∞ greater than four, both $p_{\max}$ and $y_{\max}$ are larger. In the unsteady flow the term $-\phi_t$ in Bernoulli's equation (4) contributes positively to the pressure at any point, whereas the term $-\frac{1}{2}\mathbf{v}^2$ can only act relatively to reduce the pressure.

Can we find a time scale t_F for the flip-through process? Suppose t_1 is the instant at which the spatial maximum in pressure, $p_{\max}(t)$, has *increased* to $\frac{1}{2}p_{\rm pk}$, and that t_2 is the later instant at which $p_{\max}$ has *decreased* to $\frac{1}{2}p_{\rm pk}$. (The two maxima are separated in space as well as time, as indicated in Fig. 5; the pressure at a fixed point may double and halve in a time much shorter than $t_2 - t_1$.) We define the flip-through time as $t_F = t_2 - t_1$. From (38) and (39) we find that the above instants correspond to particular values of w, which are $w = w_1 = 0.130398$ for t_1, and $w = w_2 = -1.8360$ for t_2. Equation (32) gives

$$t_F = t_2 - t_1 = 2.365\,\frac{(b - F_0)^{q_2+q_3}}{(a - F_0)^{q_1+q_3}}. \tag{43}$$

Equations (28) and (43) show that t_F decreases as V_∞ increases. We deduce that the larger the value chosen for V_∞, the more violent is the flow, in the sense that the maximum acceleration is greater and the peak pressure is higher (and the significant pressure is exerted over a shorter time-interval).

It has been suggested that the peak pressure might coincide with the time of maximum acceleration of Q. Longuet-Higgins [3] found a flow possessing an inertial shock in which free-surface acceleration and the maximum pressure pass through singularities simultaneously. However, for the present class of flows, the peak pressure occurs a short time before the maximum acceleration. A straightforward calculation shows that Q has maximum acceleration $\mathrm{d}V/\mathrm{d}t$ when $w = w_A = -0.30902$. This is less than $w_p = -0.229155$, hence the greatest acceleration is later than the peak pressure. The maximum acceleration is

$$\left.\frac{\mathrm{d}V}{\mathrm{d}t}\right|_{\max} = 0.3695\,\frac{(a - F_0)^{2q_3-q_1}}{(b - F_0)^{2q_3-q_2}}. \tag{44}$$

4 Discussion

The formula (39) suggests that high pressures can be associated with relatively small values of ${V_0}^*$, provided V_∞ is large enough. Suppose a water jet accelerates from an initial speed of ${V_0}^*$m/s to an ultimate speed of ${V_\infty}^*$m/s. This comes from a flow where the peak pressure, in N/m^2, is

$${p_{\rm pk}}^* = 0.05637\,\rho {V_0^*}^2\,\frac{{V_\infty^*}^2}{{V_0^*}^2} = 0.05637\,\rho {V_\infty^*}^2, \tag{45}$$

where the choice of F_0 for the initial free surface $y^* = F_0 {x^*}^2/{L_0}^*$, is related to the value of $V_\infty^* = V_0^*((a - F_0)/(b - F_0))^{q_3}$.

We consider a numerical example in which the velocity field varies on a length scale equal to a certain significant thickness or wavelength scale of water, say ${L_0}^* = 0.1$ m for a laboratory-scale wave. Then a velocity scale (based on deep-water linear wave theory) is ${V_0}^* = \sqrt{g{L_0}^*} = 1$ m/s. Now suppose the initial radius of curvature of the free surface at Q is $R^* = 0.2570$ m, so that the dimensionless value of $F_0 = {L_0}^*/(2R^*) = 0.1945$. Then $V_\infty = 30.41$. The peak pressure is then ${p_{\rm pk}}^* = 52\,130$ N/m^2, which is about half atmospheric pressure—not unusual for impacts at this laboratory scale. When $V_\infty = 30.41$, Eq. (44) the maximum acceleration is $\mathrm{d}V^*/\mathrm{d}t^* = 601.5$ m/s^2, which is *sixty g*. (Although $\mathrm{Fr}^{-2} = 1$ for the initial data of this example, the acceleration $\mathrm{d}V/\mathrm{d}t$ greatly exceeds Fr^{-2}, in (14) and (15), throughout the period of the key events of flip-through.)

Now suppose we repeat the calculation, but with a 0.1 mm reduction in the choice of the initial radius of curvature: suppose $R^* = 0.2569$ m. This increases F_0 to the upper limit for Type IV flip-through flows, of $F_0 = 0.1946 = b$,

for which V_∞ is singular, and hence in (30) ${p_{\rm pk}}^*$ and the acceleration are singular. This shows some extreme sensitivity of the peak pressure to the choice of initial conditions.

Flip-through occurs in a time of $t_F^* = t_F\, L_0^*/V_0^*$ seconds. Taking the earlier example, in which ${L_0}^* = 0.1\,$m, $V_0^* = 1\,$m/s, and $R^* = 0.2570\,$m, we have $V_\infty = 30.41$, so that (43) gives $t_F^* = 0.00311\,$s. Twice t_F^* is an estimate of the duration of the significant pressure 'spike' on a record of the pressure as a function of time at a fixed point on the y-axis. Here $2t_F^* = 6.2\,$ms, which is at the high end of the range of reported laboratory measurements of impact time, for water waves at this scale. Figure 5 shows that at a fixed value of y the pressure can rise and fall much quicker than the time scale for the changes in $p_{\rm max}$. So it is not surprising that $2t_F$ is longer than the duration of a typical pressure spike measured at a fixed point in an experiment. See [28] for a discussion of the impact time at different scales of water waves in both salt and fresh water.

5 Conclusions

A time-dependent velocity potential for two-dimensional flow has been shown to have local properties suitable for describing the emergence and growth of an inviscid liquid jet, in the absence of gravity or surface tension. By taking one half of the symmetric domain, the model equally well describes the frictionless advance of a liquid spreading over an impermeable plane surface, with a contact angle of ninety degrees. The family of Type IV solutions is parameterised by F_0, or equivalently by the long-time asymptotic speed of the jet nose $V_\infty > 1.695$, for which the free surface is a parabola that changes from concave to convex. This resembles the flip-through behaviour observed in some previous wave-splash computations.

The sequence of physically important events for a Type IV flow is as follows. As $t \to -\infty$ the free surface is flat. As t increases, Q accelerates, the free surface becomes concave, and the radius of curvature $1/(2F)$ at Q decreases from infinity to a local minimum given by (35). Next the radius of curvature increases to infinity as the free surface becomes flat. The surface is subsequently convex, and it has now flipped through. Next the spatial maximum in pressure $p_{\rm max}$ reaches its highest value of $p_{\rm pk}$ given by (39). The position of this peak pressure is close to Q, and the separation distance is given by Eq. (41). A little after the time of peak pressure, the acceleration of Q reaches its maximum, as given by Eq. (44). As $t \to \infty$ the velocity of Q approaches V_∞, the acceleration decays to zero, the local maximum $p_{\rm max}$ in pressure declines towards zero, and the convex free surface at Q has ever higher curvature directly proportional to $t^{3.423}$.

If we make the flow more violent by choosing ever larger V_∞ (i.e., choosing F_0 ever closer to b), then the flip-through time decreases towards zero, and both the peak pressure and the maximum acceleration increase without bound.

Further investigations are underway for nonzero Fr^{-2} and p_∞. The technologically important problem of an axisymmetric jet, can be treated using the present method. Let r be the radial distance from the y-axis of axisymmetry. The paraboloidal free surface is locally $y = Y(t) + r^2 F(t)$ and the local velocity potential in cylindrical polars is

$$\phi(r, y, t) = V(t)L(t)J_0(r/L(t))\exp([y - Y(t)]/L(t)), \tag{46}$$

where J_0 is the Bessel function of order zero, and the functions of time in (46) are different from those found in the present paper.

Acknowledgments The author dedicates this paper to the memory of Howell Peregrine who coined the term *flip-through*. The author also thanks A.A. Korobkin and the anonymous referees for their careful reading and their stimulating comments on earlier drafts.

References

1. Cooker MJ, Peregrine DH (1993) Impact pressures due to near breaking waves. In: Banner ML, Grimshaw RHJ (eds) IUTAM Symp. Breaking Waves. Springer, pp 291–297
2. Tuck EO (2000) Numerical solution for unsteady two-dimensional free surface flows. In: Miloh T, Zilman G (eds) 15th International Workshop on Water Waves and Floating Bodies. Caesarea, Israel, pp 174–177

3. Longuet-Higgins MS (2001) Vertical jets from standing waves: the bazooka effect. Proc R Soc Lond A457:495–510
4. Longuet-Higgins MS, Dommermuth DG (2001) Vertical jets from standing waves. II. Proc R Soc Lond A457:2137–2149
5. Shaw LL, Muelder SA, Baum DW, Winer KA (1994) Hypervelocity explosive-driven metal jet in air. Phys Fluids 6(9):510
6. Taylor GI (1943) A formulation of Mr. Tuck's conception of Munroe jets. In: Batchelor GK (ed) The scientific papers of Sir Geoffrey Ingram Taylor, vol 3. 358–362
7. Birkhoff G, MacDougall DP, Pugh EM, Taylor GI (1948) Explosives with lined cavities. J Appl Phys 19:563–582
8. Birkhoff G, Zarantonello EH (1957) Jets wakes and cavities. Academic, New York
9. Gurevich MI (1965) Theory of jets in ideal fluids. Academic, New York
10. Cooker MJ (2002) Unsteady pressure fields which precede the launch of free surface liquid jets. Proc R Soc Lond A458:473–488
11. Duchemin L, Josserand C, Clavin P (2005) Asymptotic behavior of the Rayleigh-Taylor instability. Phys Rev Lett 94: 224–501
12. Duchemin L (2008) Self-focusing of thin liquid jets. Proc R Soc Lond A464:197–206
13. Howison SD, Ockendon JR, Wilson SH (1991) Incompressible water-entry at small dead-rise angles. J Fluid Mech 222:215–230
14. Fraenkel LE, McLeod JB (1997) Some results for the entry of a blunt wedge into water. Phil Trans R Soc Lond A355:523–535
15. Semenov YA, Iafrati A (2006) On the nonlinear water entry problem of asymmetric wedges. J Fluid Mech 547:231–256
16. Korobkin AA (1995) Impact of two bodies one of which is covered by a thin layer of liquid. J Fluid Mech 300:43–58
17. Howison SD, Ockendon J, Oliver JM, Purvis R, Smith FT (2005) Droplet impact on a thin fluid layer. J Fluid Mech 542:1–23
18. Borisova EP, Koriavov PP, Moiseev NN (1959) Plane and axially symmetric similarity problems of penetration and of stream impact. J Appl Math Mech 23:490–507
19. Zeff BW, Kleber B, Fineberg J, Lathrop DP (2000) Singularity dynamics in curvature collapse and jet eruption on a fluid surface. Nature 403:401–404
20. Roisman IV, Tropea C (2002) Impact of a drop onto a wetted wall: description of crown formation and propagation. J Fluid Mech 472:373–397
21. Korobkin AA, Scolan Y-M (2006) Three-dimensional theory of water impact. Part 2. Linearized Wagner problem. J Fluid Mech 549:373–434
22. Longuet-Higgins MS, Oguz H (1995) Critical microjets in collapsing cavities. J Fluid Mech 290:183–201
23. Korobkin AA, Yilmaz O (2009) The initial stage of dam-break flow. J Eng Math 63:293–308
24. King AC, Needham DJ (1994) The initial development of a jet caused by fluid, body and free-surface interaction. I. A uniformly accelerating plate. J Fluid Mech 268:89–101
25. Shu J-J (2004) Impact of an oblique breaking wave on a wall. Phys Fluids 16(3):1–42
26. Needham DJ, Chamberlain PG, Billingham J (2008) The initial development of a jet caused by fluid, body and free-surface interaction. Part 3. An inclined accelerating plate. Q J Mech Appl Math 61:581–614
27. Bagnold RA (1939) Interim report on wave pressure research. Proc Inst Civ Eng 12:201–226
28. Bullock GN, Obhrai C, Peregrine DH, Bredmose H (2007) Violent breaking wave impacts. Part 1: results from large-scale regular wave tests on vertical and sloping walls. Coast Eng 54:602–617